

# UC Santa Barbara

## UC Santa Barbara Previously Published Works

### Title

Two-dimensional electron gas in a modulation-doped SrTiO<sub>3</sub>/Sr(Ti, Zr)O<sub>3</sub> heterostructure

### Permalink

<https://escholarship.org/uc/item/76h8g79f>

### Journal

Applied Physics Letters, 103(8)

### Authors

Kajdos, Adam P.  
Ouellette, Daniel G.  
Cain, Tyler A.  
et al.

### Publication Date

2013-08-23

### DOI

10.1063/1.4819203

Peer reviewed

## Two-dimensional electron gas in a modulation-doped SrTiO<sub>3</sub>/Sr(Ti, Zr)O<sub>3</sub> heterostructure

Adam P. Kajdos,<sup>1</sup> Daniel G. Ouellette,<sup>2</sup> Tyler A. Cain,<sup>1</sup> and Susanne Stemmer<sup>1</sup>

<sup>1</sup>Materials Department, University of California, Santa Barbara, California 93106-5050, USA

<sup>2</sup>Department of Physics, University of California, Santa Barbara, California 93106-9530, USA

(Received 30 June 2013; accepted 9 August 2013; published online 23 August 2013)

A two-dimensional electron gas (2DEG) in SrTiO<sub>3</sub> is created via modulation doping by interfacing undoped SrTiO<sub>3</sub> with a wider-band-gap material, SrTi<sub>1-x</sub>Zr<sub>x</sub>O<sub>3</sub>, which is doped n-type with La. All layers are grown using hybrid molecular beam epitaxy. Using magnetoresistance measurements, we show that electrons are transferred into the SrTiO<sub>3</sub>, and a 2DEG is formed. In particular, Shubnikov-de Haas oscillations are shown to depend only on the perpendicular magnetic field. Experimental Shubnikov-de Haas oscillations are compared with calculations that assume multiple occupied subbands. © 2013 AIP Publishing LLC. [<http://dx.doi.org/10.1063/1.4819203>]

Two-dimensional electron gases (2DEGs) at interfaces between SrTiO<sub>3</sub> and other complex oxides exhibit unique phenomena, including superconductivity,<sup>1</sup> Rashba spin-orbit coupling,<sup>2</sup> and magnetism.<sup>3-7</sup> Most studies thus far have focused on 2DEGs at polar/nonpolar interfaces, such as LaAlO<sub>3</sub>/SrTiO<sub>3</sub>,<sup>8-10</sup> LaTiO<sub>3</sub>/SrTiO<sub>3</sub>,<sup>11,12</sup> and GdTlO<sub>3</sub>/SrTiO<sub>3</sub>.<sup>13,14</sup> Mobile carriers in these heterostructures arise from a polar discontinuity at the interface, which gives rise to extremely high carrier densities on the order of  $\sim 3 \times 10^{14} \text{ cm}^{-2}$  (LaAlO<sub>3</sub>/SrTiO<sub>3</sub> interfaces typically have lower densities, for reasons that are not yet well understood<sup>9</sup>). An alternative route to high-mobility 2DEGs is modulation doping, originally developed for III-V heterostructures,<sup>15</sup> leading to devices such as high-electron mobility transistors,<sup>16,17</sup> and scientific discoveries, such as the fractional quantum Hall effect.<sup>18</sup> This approach spatially separates the mobile charge from the ionized dopants by transferring it into an undoped layer. A heterostructure that has suitable conduction band alignments is therefore essential for modulation doping.

Here, we show that a 2DEG in SrTiO<sub>3</sub> can be created by modulation doping. We use SrTi<sub>1-x</sub>Zr<sub>x</sub>O<sub>3</sub> as the doped, wider band gap perovskite, i.e., the analog of AlGaAs in GaAs/AlGaAs structures. SrTi<sub>1-x</sub>Zr<sub>x</sub>O<sub>3</sub> is a solid solution of cubic SrTiO<sub>3</sub> and orthorhombic SrZrO<sub>3</sub>. The band gap of SrZrO<sub>3</sub> (5.6 eV (Ref. 19)) is substantially larger than that of SrTiO<sub>3</sub> (3.2 eV). The band alignment between SrTiO<sub>3</sub> and SrZrO<sub>3</sub> is Type I, with a conduction band offset,  $\Delta E_c$ , of 1.9 eV.<sup>20</sup> Given the large  $\Delta E_c$ , reasonable band offsets should be achievable even for small  $x$ , which serve to reduce the substantial lattice mismatch between SrTiO<sub>3</sub> ( $a = 3.905 \text{ \AA}$ ) and SrZrO<sub>3</sub> (pseudocubic unit cell,  $a \approx 4.1 \text{ \AA}$ ), and facilitate doping, which would likely be difficult in a wide band gap material such as SrZrO<sub>3</sub>.

Figure 1 shows a sketch of a modulation doped SrTiO<sub>3</sub>/SrTi<sub>0.95</sub>Zr<sub>0.05</sub>O<sub>3</sub> heterostructure, along with a band diagram of the conduction band edge, Fermi level and the electron density, as calculated using a 1D Poisson solver.<sup>21</sup> A  $\Delta E_c$  of 95 meV was estimated using Vegard's law. The SrTi<sub>0.95</sub>Zr<sub>0.05</sub>O<sub>3</sub> layer is n-type, doped with La to a carrier density of  $2 \times 10^{19} \text{ cm}^{-3}$ . A 2DEG resides in the SrTiO<sub>3</sub>.

Experimentally realizing this structure requires the growth of epitaxial, stoichiometric SrTiO<sub>3</sub> and SrTi<sub>1-x</sub>Zr<sub>x</sub>O<sub>3</sub>

thin films, to ensure high mobility, avoid charge trapping, and allow for doping of the SrTi<sub>1-x</sub>Zr<sub>x</sub>O<sub>3</sub>. Here, we use hybrid molecular beam epitaxy (MBE), previously developed for high-mobility SrTiO<sub>3</sub>.<sup>22,23</sup> In this approach, both Ti and Zr are supplied from high-purity (99.999%) metal-organic precursors, titanium tetra isopropoxide (TTIP), and zirconium tert-butoxide (ZTB), respectively.

The SrTi<sub>0.95</sub>Zr<sub>0.05</sub>O<sub>3</sub>/SrTiO<sub>3</sub> heterostructure discussed in this paper consists of a 120 nm undoped SrTiO<sub>3</sub> layer grown on (001) SrTiO<sub>3</sub>, followed by growth of a 30-nm-thick La-doped SrTi<sub>0.95</sub>Zr<sub>0.05</sub>O<sub>3</sub> layer (see Fig. 1). For SrTi<sub>1-x</sub>Zr<sub>x</sub>O<sub>3</sub>, both precursors were co-evaporated, and the beam equivalent pressures were adjusted relative to

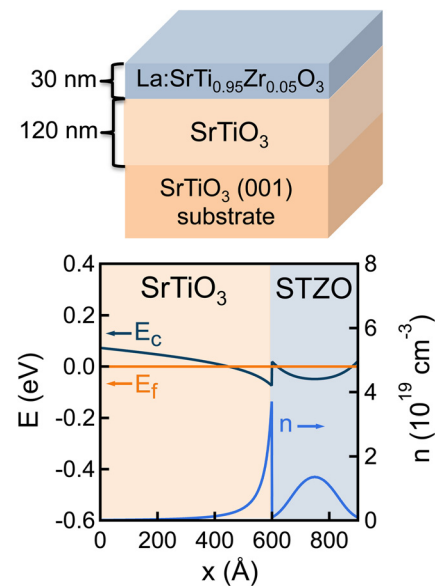


FIG. 1. Schematic of a modulation-doped SrTi<sub>0.95</sub>Zr<sub>0.05</sub>O<sub>3</sub>/SrTiO<sub>3</sub> heterostructure and corresponding band diagram. The conduction band offset was estimated using experimental values for SrZrO<sub>3</sub>/SrTiO<sub>3</sub> (Ref. 20) and assuming Vegard's law. The conduction band edge ( $E_c$ ), Fermi level ( $E_f$ ), and carrier density ( $n$ ) were calculated using a 1D Poisson solver.<sup>21</sup> The dopant density in the SrTi<sub>0.95</sub>Zr<sub>0.05</sub>O<sub>3</sub> and the surface pinning potential were assumed to be  $2 \times 10^{19} \text{ cm}^{-3}$  and 0.1 eV, respectively. The SrTiO<sub>3</sub> layer is nominally undoped with  $\sim 10^{16} \text{ cm}^{-3}$  residual donor-type defects (an upper limit established by doping studies for these high-quality MBE films).

that of Sr to give A:B site stoichiometric films (where A = Sr and B = Ti or Zr) of the desired Zr content ( $x$ ). Growth optimization to obtain the correct A:B site ratio closely followed our approach for SrTiO<sub>3</sub>,<sup>23</sup> and details will be reported elsewhere. Oxygen was supplied by an rf plasma source. The substrate temperature was 900 °C as measured by thermocouple. La was evaporated from a solid source effusion cell to obtain a carrier concentration of  $2 \times 10^{19} \text{ cm}^{-3}$ . Doping calibrations were carried out using thick, uniformly doped layers, which confirmed  $n$ -type doping of the SrTi<sub>0.95</sub>Zr<sub>0.05</sub>O<sub>3</sub> layers, but showed much lower mobilities than the modulation doped samples investigated here. *In-situ* reflection high-energy diffraction (RHEED) patterns were streaky during and after growth for all films and showed periodic oscillations in intensity at the beginning of growth, indicating layer-by-layer growth.<sup>24</sup>  $2\theta$ - $\omega$  x-ray diffraction scans in the vicinity of the SrTiO<sub>3</sub> 002 reflection showed a single, separate 002 peak for the SrTi<sub>1-x</sub>Zr<sub>x</sub>O<sub>3</sub> film and clearly defined Laue oscillations.<sup>24</sup> The composition  $x$  was calibrated by comparing the unstrained unit cell volume, obtained from lattice parameter measurements, to that of bulk SrTi<sub>1-x</sub>Zr<sub>x</sub>O<sub>3</sub>.<sup>25</sup> The sample was post-growth annealed in a rapid thermal annealing furnace in 1 atm of oxygen at 800 °C for 30 s to ensure oxygen stoichiometry. Hall and longitudinal resistance measurements at temperatures between 300 K and 2 K and magnetic fields ( $B$ ) up to 14 T were performed in van der Pauw geometry using a Physical Properties Measurement System (Quantum Design). Ohmic contacts (40 nm-Al/20 nm-Ni/400 nm-Au) were deposited by electron beam evaporation through a shadow mask onto the corners of a square sample. The longitudinal magnetoresistance was measured using a standard lock-in technique in a He<sup>3</sup> cryostage at temperatures ranging from 0.45 K to 3 K. Data at low  $B$  showed positive magnetoresistance at low temperatures, with a sharp dip near  $B=0$ , possibly due to weak antilocalization. Magnetoresistance measurements as a function of the angle  $\theta$  that  $B$  makes with the surface normal were performed at 2 K using a horizontal sample rotator stage ( $\theta=0^\circ$  indicates that  $B$  is perpendicular to the interface).

To confirm the existence of a 2DEG and to probe the dimensionality of the electron system in the SrTi<sub>0.95</sub>Zr<sub>0.05</sub>O<sub>3</sub>/SrTiO<sub>3</sub> heterostructure, we investigate Shubnikov-de Haas oscillations that appear in the longitudinal magnetoresistance in a quantizing magnetic field. In particular, for a 2DEG, the periodicity of these oscillations, which are due to quantization into Landau levels, should only depend on the component of  $B$  that is normal to the interface.

Figure 2 shows the longitudinal magnetoresistance at different temperatures. At 0.45 K, Shubnikov-de Haas oscillations are observed for  $B > 5$  T. Oscillations persist to temperatures up to 3 K. The oscillating component of the magnetoresistance,  $\Delta R_{xx}$ , was obtained by subtracting the non-oscillating background using multiple polynomial fits. Figure 3(a) shows  $\Delta R_{xx}$  as a function of  $1/B$  [ $\Delta R_{xx}(1/B)$ ] at 0.45 K. A Fourier transform (FT) of  $\Delta R_{xx}(1/B)$  is shown in the inset and exhibits multiple peaks, which will be further discussed below. Figure 3(b) shows Shubnikov-de Haas oscillations for different  $\theta$ , measured at 2 K and plotted against  $(B \cos \theta)^{-1}$ . Resistance maxima and minima appear

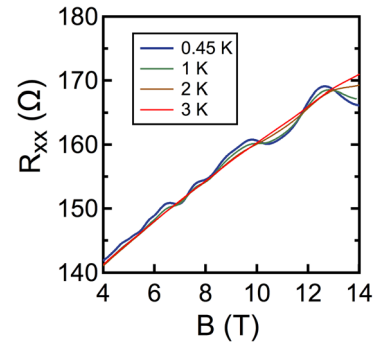


FIG. 2. Longitudinal magnetoresistance ( $R_{xx}$ ) measured at temperatures between 0.45 K and 3 K.

at the same values of  $(B \cos \theta)^{-1}$  for  $\theta$  up to  $60^\circ$ , confirming the two-dimensionality of the electron system. Therefore, as suggested by the band diagram in Fig. 1, a 2DEG has been created on the SrTiO<sub>3</sub>-side of the interface.

Shubnikov-de Haas oscillations allow for the extraction of important characteristics, including the effective masses ( $m^*$ ) for the subbands and the quantum scattering time ( $\tau_q$ ) or Dingle temperature ( $T_D$ ). For 2DEGs with a single subband, values for  $m^*$  and  $T_D$  are determined from the decay in the amplitude of oscillations with increasing temperature and by constructing a Dingle plot at a fixed temperature, respectively. Multiple subbands (or spin splitting) complicate such analyses, since oscillations contain contributions from several components. Therefore, we fit the experimental data,  $\Delta R_{xx}(1/B)$ , at 0.45 K to the standard equation<sup>26</sup>

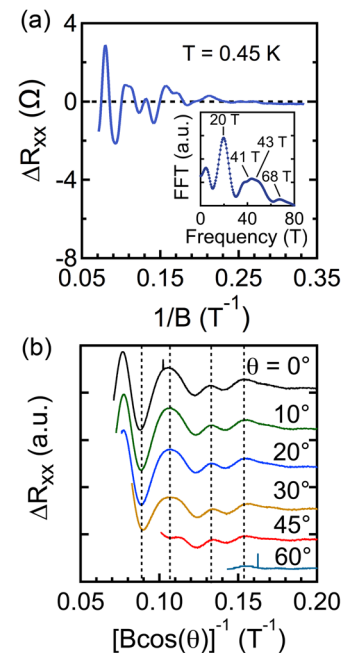


FIG. 3. (a) Shubnikov-de Haas oscillations,  $\Delta R_{xx}(1/B)$ , measured at 0.45 K and  $\theta=0^\circ$ . The inset shows a Fourier transform of the data. Approximate positions for four peaks are labeled. (b) Shubnikov-de Haas oscillations measured at 2 K at various tilt angles  $\theta$  (the angle between  $B$  and the interface plane normal) and plotted as a function of the inverse perpendicular component of the magnetic field,  $(B \cos \theta)^{-1}$ .

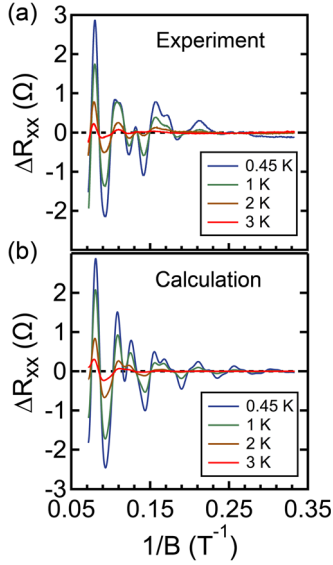


FIG. 4. (a) Temperature-dependent Shubnikov-de Haas oscillations,  $\Delta R_{xx}(1/B)$ , measured at  $\theta = 0^\circ$  and at temperatures between 0.45 K and 3 K. (b) Calculated [Eq. (1)] Shubnikov-de Haas oscillations for temperatures between 0.45 K and 3 K, using the parameters listed in Table I.

$$\frac{\Delta R_{xx}}{R_0} = \sum_{i=1}^l 2A_i \exp\left(-\frac{2\pi^2 k_B T_{D,i}}{\hbar\omega_c}\right) \frac{X}{\sinh(X)} \cos\left(\frac{2\pi f_i}{B} + \pi\right), \quad (1)$$

where  $i$  is the subband index,  $l$  is the number of occupied subbands,  $A_i$  are amplitude factors associated with intrasubband scattering probabilities,  $k_B$  is the Boltzmann constant,  $T_{D,i}$  is the Dingle temperature of each subband,  $\hbar$  is the reduced Planck's constant,  $\omega_c$  is the cyclotron frequency,  $f_i$  are the oscillation frequencies (in  $1/B$ ), and  $X = (2\pi^2 k_B T)/(\hbar\omega_c)$ . Figure 4 shows experimental and calculated  $\Delta R_{xx}(1/B)$  at temperatures between 0.45 K and 3 K for  $l = 4$ . The temperature-dependence was calculated and the  $m^*$ 's adjusted to match the experimentally observed behavior. The parameters obtained from the fits and the extracted sheet carrier density ( $n_s$ ),  $\tau_q$ , and quantum mobility ( $\mu_q$ ) for each subband are shown in Table I. The frequencies are in good agreement with those obtained in the FTs shown in Fig. 3(a). The lowest value for  $m^*$  (0.95  $m_0$ , where  $m_0$  is the free electron mass) is consistent with a  $d_{xy}$ -derived subband.<sup>27–30</sup> Spin-orbit coupling can hybridize  $d_{xy}$ -derived with  $d_{xz}/d_{yz}$ -derived subbands.<sup>29</sup> This results in a heavier in-plane mass. Theoretical calculations support multiple occupied subbands at this carrier density.<sup>29</sup> Alternative models and fits to the experimental Shubnikov-de Haas oscillations were also

explored (see Ref. 24), including whether multiple frequencies could arise from two spin-split subbands. A good qualitative match with the data could be obtained, and at present, we cannot distinguish between these models.<sup>24</sup> These uncertainties place limitations on the accuracy of the extracted values in Table I. The extracted  $\mu_q$ 's of around  $2000 \text{ cm}^2 \text{V}^{-1} \text{s}^{-1}$  are consistent with the onset of magnetoresistance oscillations around 4–5 T, i.e., when  $\mu_q B > 1$ .

The total sheet density estimated from Table I is approximately  $8.4 \times 10^{12} \text{ cm}^{-2}$ , which is only 19% the Hall density,  $n_{s,H} = 4.46 \times 10^{13} \text{ cm}^{-2}$ , measured at 300 K. The remaining carriers can be reasonably assumed to reside in the La-doped  $\text{SrTi}_{0.95}\text{Zr}_{0.05}\text{O}_3$  layer. Carrier distributions calculated in Fig. 1 confirm this picture qualitatively. Using reasonable assumptions for the mobilities and carrier densities in both layers, a Hall coefficient can be calculated from a multi-carrier model and compared with experimentally measured values. Good agreement is found.<sup>24</sup> The two spin-split subband interpretation of the data (see Ref. 24) results in lower carrier densities. Prior studies of 2DEGs in  $\text{SrTiO}_3$  found upwards of 60%–95% of carriers in the 2DEG to not give rise to oscillations,<sup>14,31–34</sup> which is likely due to disorder limiting the mobility of a significant fraction of the carriers, preventing oscillations to be resolved for all subbands.

Discrepancies exist between calculated and experimental  $\Delta R_{xx}$  in all models. One possible explanation is intersubband scattering,<sup>35,36</sup> which was neglected in Eq. (1). The energy spacing between subbands,  $\Delta E$ , is very small

$$\Delta E = \frac{q\hbar\Delta f}{m^*}, \quad (2)$$

where  $\Delta f$  is the difference in oscillation frequencies between any two subbands, and  $q$  is the elementary charge. From Table I,  $\Delta E$  ranges from 0.15 meV to 5 meV. Intersubband scattering may thus be significant. It is generally more significant at low  $B$ <sup>35,36</sup> and could thus potentially affect finer features that would otherwise appear in the measured resistance. At present, a complete theory of magnetoresistance oscillations of 2DEGs in  $\text{SrTiO}_3$  is still lacking.

In summary, we have shown that modulation doping provides an alternative route to 2DEGs in  $\text{SrTiO}_3$ . Future studies should be dedicated to a complete understanding of the quantum oscillations, and to further improving the mobility in these structures. For example, remote ionized impurity scattering can be mitigated by inserting an undoped  $\text{SrTi}_{1-x}\text{Zr}_x\text{O}_3$  spacer. Lower-density 2DEGs can be obtained by optimizing the doping and Zr content of the  $\text{SrTi}_{1-x}\text{Zr}_x\text{O}_3$ , which determine the band offsets.

TABLE I. Parameters extracted from fits of the experimental Shubnikov-de Haas oscillations measured at 0.45 K to a four-subband model [Eq. (1)]. Also shown are the sheet carrier densities ( $n_s$ ), quantum scattering times ( $\tau_q$ ), and quantum mobilities ( $\mu_q$ ) of each subband extracted from the fits. The effective mass  $m^*$  is determined from the cyclotron frequency  $\omega_c = eB/m^*$ ,  $\tau_q$  is calculated from  $\tau_q = \hbar/(2\pi k_B T_D)$ , and  $n_s$  is calculated from  $f = nh/2q$ , where  $h$  is Planck's constant.

Subband index $i$	$R_0 A$ ( $\Omega$ )	$f$ (T)	$m^*$ ( $m_0$ )	$T_D$ (K)	$n_s$ ( $\text{cm}^{-2}$ )	$\tau_q$ (s)	$\mu_q$ ( $\text{cm}^2 \text{V}^{-1} \text{s}^{-1}$ )
1	0.8	68.4	1.2	0.8	$3.30 \times 10^{12}$	$1.52 \times 10^{-12}$	2225
2	6.5	43	1.5	1.1	$2.08 \times 10^{12}$	$1.10 \times 10^{-12}$	1288
3	2	41.2	1.4	0.8	$1.99 \times 10^{12}$	$1.52 \times 10^{-12}$	1907
4	2	21.2	0.95	0.9	$1.02 \times 10^{12}$	$1.35 \times 10^{-12}$	2496

The authors thank David Awschalom for making available the equipment for magnetotransport measurements and Jim Allen, Guru Khalsa, and Allan MacDonald for helpful discussions. A.P.K. and T.A.C. received support from the National Science Foundation through a Graduate Research Fellowship (Grant No. DGE-1144085) and the Department of Defense through a NDSEG fellowship, respectively. Experimental costs (A.P.K.) were supported by the UCSB MRL, which is supported by the MRSEC Program of the National Science Foundation under Award No. DMR-1121053 and (T.A.C.) by the Center for Energy Efficient Materials, an Energy Frontier Research Center funded by the DOE (Award No. DESC0001009). The work also made use of the UCSB Nanofabrication Facility, a part of the NSF-funded NNIN network.

- <sup>1</sup>N. Reyren, S. Thiel, A. D. Caviglia, L. F. Kourkoutis, G. Hammerl, C. Richter, C. W. Schneider, T. Kopp, A. S. Ruetschi, D. Jaccard *et al.*, *Science* **317**, 1196 (2007).
- <sup>2</sup>A. D. Caviglia, M. Gabay, S. Gariglio, N. Reyren, C. Cancellieri, and J. M. Triscone, *Phys. Rev. Lett.* **104**, 126803 (2010).
- <sup>3</sup>A. Brinkman, M. Huijben, M. Van Zalk, J. Huijben, U. Zeitler, J. C. Maan, W. G. Van der Wiel, G. Rijnders, D. H. A. Blank, and H. Hilgenkamp, *Nature Mater.* **6**, 493 (2007).
- <sup>4</sup>J. A. Bert, B. Kalisky, C. Bell, M. Kim, Y. Hikita, H. Y. Hwang, and K. A. Moler, *Nat. Phys.* **7**, 767 (2011).
- <sup>5</sup>L. Li, C. Richter, J. Mannhart, and R. C. Ashoori, *Nat. Phys.* **7**, 762 (2011).
- <sup>6</sup>P. Moetakef, J. R. Williams, D. G. Ouellette, A. P. Kajdos, D. Goldhaber-Gordon, S. J. Allen, and S. Stemmer, *Phys. Rev. X* **2**, 021014 (2012).
- <sup>7</sup>D. A. Dikin, M. Mehta, C. W. Bark, C. M. Folkman, C. B. Eom, and V. Chandrasekhar, *Phys. Rev. Lett.* **107**, 056802 (2011).
- <sup>8</sup>A. Ohtomo and H. Y. Hwang, *Nature* **427**, 423 (2004).
- <sup>9</sup>M. Huijben, A. Brinkman, G. Koster, G. Rijnders, H. Hilgenkamp, and D. H. A. Blank, *Adv. Mater.* **21**, 1665 (2009).
- <sup>10</sup>J. Mannhart, D. H. A. Blank, H. Y. Hwang, A. J. Millis, and J. M. Triscone, *MRS Bull.* **33**, 1027 (2008).
- <sup>11</sup>A. Ohtomo, D. A. Muller, J. L. Grazul, and H. Y. Hwang, *Nature* **419**, 378 (2002).
- <sup>12</sup>J. S. Kim, S. S. A. Seo, M. F. Chisholm, R. K. Kremer, H. U. Habermeier, B. Keimer, and H. N. Lee, *Phys. Rev. B* **82**, 201407 (2010).
- <sup>13</sup>P. Moetakef, T. A. Cain, D. G. Ouellette, J. Y. Zhang, D. O. Klenov, A. Janotti, C. G. Van de Walle, S. Rajan, S. J. Allen, and S. Stemmer, *Appl. Phys. Lett.* **99**, 232116 (2011).
- <sup>14</sup>P. Moetakef, D. G. Ouellette, J. R. Williams, S. J. Allen, L. Balents, D. Goldhaber-Gordon, and S. Stemmer, *Appl. Phys. Lett.* **101**, 151604 (2012).
- <sup>15</sup>R. Dingle, H. L. Stormer, A. C. Gossard, and W. Wiegmann, *Appl. Phys. Lett.* **33**, 665 (1978).
- <sup>16</sup>T. Mimura, S. Hiyamizu, T. Fujii, and K. Nanbu, *Jpn. J. Appl. Phys., Part 2* **19**, L225 (1980).
- <sup>17</sup>D. Delagebeaudeuf and N. T. Linh, *IEEE Trans. Electron Devices* **29**, 955 (1982).
- <sup>18</sup>D. C. Tsui, H. L. Stormer, and A. C. Gossard, *Phys. Rev. Lett.* **48**, 1559 (1982).
- <sup>19</sup>Y. S. Lee, J. S. Lee, T. W. Noh, D. Y. Byun, K. S. Yoo, K. Yamaura, and E. Takayama-Muromachi, *Phys. Rev. B* **67**, 113101 (2003).
- <sup>20</sup>R. Schafranek, J. D. Baniecki, M. Ishii, Y. Kotaka, K. Yamanka, and K. Kurihara, *J. Phys. D: Appl. Phys.* **45**, 055303 (2012).
- <sup>21</sup>M. Grundmann, BandEng program.
- <sup>22</sup>J. Son, P. Moetakef, B. Jalan, O. Bierwagen, N. J. Wright, R. Engel-Herbert, and S. Stemmer, *Nature Mater.* **9**, 482 (2010).
- <sup>23</sup>B. Jalan, R. Engel-Herbert, N. J. Wright, and S. Stemmer, *J. Vac. Sci. Technol. A* **27**, 461 (2009).
- <sup>24</sup>See supplemental material at <http://dx.doi.org/10.1063/1.4819203> for additional structural data, alternative fits to the Shubnikov-de Haas data, and for an estimate of the Hall coefficient assuming 4 subbands.
- <sup>25</sup>T. K.-Y. Wong, B. J. Kennedy, C. J. Howard, B. A. Hunter, and T. Vogt, *J. Solid State Chem.* **156**, 255 (2001).
- <sup>26</sup>A. Isihara and L. Smrcka, *J. Phys. C* **19**, 6777 (1986).
- <sup>27</sup>H. Uwe, R. Yoshizaki, T. Sakudo, A. Izumi, and T. Uzumaki, *Jpn. J. Appl. Phys., Part 2* **24**(Suppl. 24-2), L335 (1985), available online <http://jap.jsap.jp/link?JJAPS/24S2/335/>.
- <sup>28</sup>P. Delugas, A. Filippetti, V. Fiorentini, D. I. Bilc, D. Fontaine, and P. Ghosez, *Phys. Rev. Lett.* **106**, 166807 (2011).
- <sup>29</sup>G. Khalsa and A. H. MacDonald, *Phys. Rev. B* **86**, 125121 (2012).
- <sup>30</sup>W. J. Son, E. Cho, B. Lee, J. Lee, and S. Han, *Phys. Rev. B* **79**, 245411 (2009).
- <sup>31</sup>Y. Kozuka, M. Kim, C. Bell, B. G. Kim, Y. Hikita, and H. Y. Hwang, *Nature* **462**, 487 (2009).
- <sup>32</sup>A. D. Caviglia, S. Gariglio, C. Cancellieri, B. Sacepe, A. Fete, N. Reyren, M. Gabay, A. F. Morpurgo, and J. M. Triscone, *Phys. Rev. Lett.* **105**, 236802 (2010).
- <sup>33</sup>B. Jalan, S. Stemmer, S. Mack, and S. J. Allen, *Phys. Rev. B* **82**, 081103 (2010).
- <sup>34</sup>Y. Z. Chen, N. Bovet, F. Trier, D. V. Christensen, F. M. Qu, N. H. Andersen, T. Kasama, W. Zhang, R. Giraud, J. Dufouleur *et al.*, *Nat. Commun.* **4**, 1371 (2013).
- <sup>35</sup>P. T. Coleridge, *Semicond. Sci. Technol.* **5**, 961 (1990).
- <sup>36</sup>T. H. Sander, S. N. Holmes, J. J. Harris, D. K. Maude, and J. C. Portal, *Phys. Rev. B* **58**, 13856 (1998).